Molecular Therapy
Original Article

Epigenetically Upregulated MicroRNA-602 Is Involved in a Negative Feedback Loop with FOXK2 in Esophageal Squamous Cell Carcinoma

Meiyue Liu,[1,4] Jiarui Yu,[1,4] Dan Wang,[1,4] Yi Niu,[1] Siyuan Chen,[1] Peng Gao,[1] Zhao Yang,[1] Huan Wang,[1] Jie Zhang,[2] Chao Zhang,[1] Yue Zhao,[3] Wanning Hu,[1] and Guogui Sun[1]

[1]Department of Radiation Oncology, North China University of Science and Technology Affiliated People's Hospital, Tangshan 063000, China; [2]Department of Pathology, North China University of Science and Technology Affiliated People's Hospital, Tangshan 063000, China; [3]Zhejiang Cancer Research Institute, Zhejiang Cancer Hospital, Hangzhou 310022, China

MicroRNA is an endogenous, small RNA controlling multiple target genes and playing roles in various tumorigenesis processes. In this study, our results revealed that miR-602 expression levels in tumor tissues and preoperative serum from esophageal squamous cell carcinoma (ESCC) patients were higher than those in non-tumorous tissues and healthy volunteers. miR-602 overexpression was closely related to lymph node metastasis and TNM stages and correlated short overall, and it acted as an independent prognostic marker of ESCC. The methylation status of the miR-602 gene indicated more frequent hypomethylation of the CpG sites located upstream of the miR-602 gene in the ESCC tissues than in the adjacent normal tissues, and the methylation status of miR-602 correlated inversely with its expression levels. Subsequently, miR-602 overexpression promoted ESCC proliferation and metastasis and regulated cell cycles *in vitro* and *in vivo*. Mechanistically, a dual-luciferase experiment validated that Fork head box (FOX)K2 (FOXK2) was a direct target of miR-602. More importantly, systemic delivery of formulated miR-602 antagomir could reduce tumor growth and increased FOXK2 protein expression in nude mice. This work provides novel insight into the molecular pathogenesis of ESCC.

INTRODUCTION

Esophageal squamous cell carcinoma (ESCC) is a serious health problem in China with 375,000 new deaths in 2015.[1] Due to the lack of typical clinical symptoms and effective techniques for early diagnosis, ESCC is typically at late stage and the 5-year survival rate is still less than 15%. Therefore, it is very important to understand the mechanisms of the occurrence and development of ESCC at the molecular level and to explore diagnostic options and effective treatment targets for early diagnosis and treatment of ESCC.[2]

MicroRNAs (miRNAs), a group of small, single-stranded non-coding RNAs with 18–25 nt in length, can negatively regulate gene expression by binding to the 3′ UTR of the corresponding target mRNAs at a post-transcriptional level.[3] Emerging evidence has demonstrated that miRNA dysfunction is involved in various physiological and pathological processes, including cell proliferation, apoptosis, drug resistance, and tumor metastasis.[4–7] miRNAs have been reported to have promising roles in cancer diagnosis, treatment, and prognosis.[8,9] Variations in the expressions of miRNAs have been identified in lung cancer tissues compared to their normal counterparts. For example, the reduced expressions of miRNAs such as miR-15a and miR-21 have been noted in two common types of non-small-cell lung cancer (NSCLC).[10] However, miR-106a, miR-146, miR-150, miR-155, miR-17-3p, miR-191, miR-197, miR-192, miR-21, miR-203, miR-205, miR-210, miR-212, and miR-214 have been reported to be upregulated in lung cancer.[11] miR-195 expression was shown to be lower in ESCC tissues and associated with poor survival outcome.[12] In colorectal cancer, high expression levels of miR-135b and low levels of miR-590-5p expression are associated with clinical stages and survival progression.[5,13]

Recently, many studies demonstrated that miRNAs were detectable in plasma or serum and could act as non-invasive biomarkers for the diagnosis or prognosis of cancer.[14,15] Endogenous circulating miRNAs have attracted significant attention regarding the diagnosis, prognosis, and metastasis of cancer. In fact, accumulating reports also suggest the potential of miRNAs in the early detection of patients with several malignancies, such as lung cancer,[16] breast cancer,[17] and gastric cancer.[18] However, the results were not consistent among the studies, partly due to different research methods and tested populations. Also, most studies only focused on some specific miRNAs,

Received 24 February 2019; accepted 8 July 2019;
https://doi.org/10.1016/j.ymthe.2019.07.006.

[4]These authors contributed equally to this work.

Correspondence: Guogui Sun, Department of Radiation Oncology, North China University of Science and Technology Affiliated People's Hospital, 65 Shengli Road, Tangshan 063000, China.
E-mail: guogui_sun2013@163.com
Correspondence: Yue Zhao, Department of Zhejiang Cancer Research Institute, Zhejiang Cancer Hospital, Hangzhou 310022, China.
E-mail: zhaoyue@zjcc.org.cn
Correspondence: Wanning Hu, Department of Radiation Oncology, North China University of Science and Technology Affiliated People's Hospital, 65 Shengli Road, Tangshan 063000, China.
E-mail: wanning_hu2008@sina.com

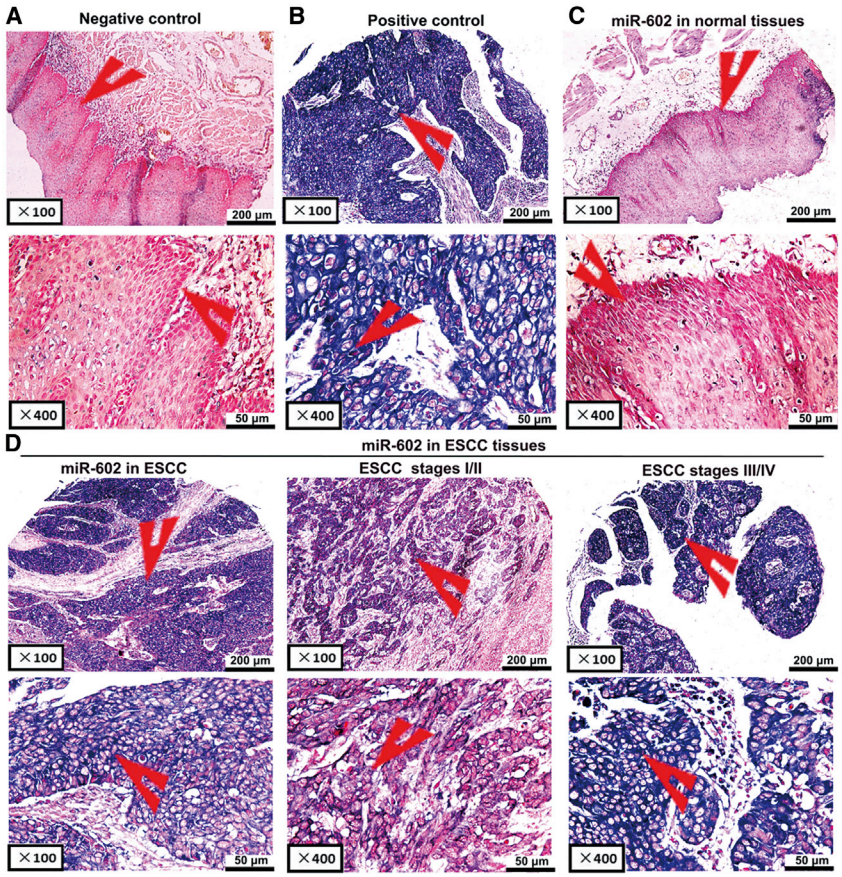

Figure 1. *In Situ* Hybridization to Detect miR-602 Expression in 93 Paired ESCC and Adjacent Non-cancerous Tissue Samples

(A) Scrambled miRNA negative control (no expression). (B) U6 snRNA positive control (strong expression). (C) miR-602 expression in adjacent esophageal tissues (no or low expression). (D) miR-602 expression in ESCC tissues (left and middle, low or moderate expression; right, strong expression).

while few studies comprehensively explored circulating miRNA profiles in ESCC.

The coding gene of miR-602 is located in chromosome region 9q34.3. The Cancer Genome Atlas (TCGA) database (https://www.cancer.gov/about-nci/organization/ccg/research/structural-genomics/) and recent research demonstrated that the expression of miR-602 was identified to be significantly upregulated in ESCC tissues. However, the biological function of miR-602 in esophageal cancer and the molecular mechanisms remain unclear. In the present study, we examined the expression status and prognostic value of miR-602 in ESCC. Particularly, the correlation between miR-602 expression and ESCC progression and the role of serum miR-602 as a non-invasive biomarker in ESCC were further evaluated. In addition, the roles of miR-602 in promoting multiple aspects of tumor development, including tumor growth and metastasis, as well as the underlying molecular mechanisms were investigated.

RESULTS

miR-602 Expression in Human ESCC Was Increased and Significantly Correlated with Poor Survival

To determine the potential functions of miR-602 in ESCC pathogenesis, we used TCGA database to analyze miR-602 expression in ESCC tissues; miR-602 was significantly upregulated in ESCC tissues compared to normal adjacent tissues (Figure S1). We further analyzed the expression of miR-602 in 93 ESCC tissue samples compared with their adjacent normal esophageal tissues. miR-602 staining was negative or weak relative to normal adjacent esophageal tissues that exhibited light to dark staining (Figure 1A). In contrast, miR-602 signals were confined to positive images in esophageal tissues (Figure 1B). *In situ* hybridization also showed that miR-602 expression was significantly upregulated in tumor tissue samples compared with control samples, especially for ESCC stages III and IV (Figures 1C and 1D; Table 1, discovery group; $p < 0.05$).

Moreover, we analyzed the relationship between clinicopathologic features and miR-602 expression levels in ESCC cases. Importantly, we found that the upregulation of miR-602 expression was associated with lymph node metastasis and advanced clinical stages (Table 1, discovery group; $p < 0.05$). Clinically, the Kaplan-Meier test indicated that patients with miR-602 overexpression exhibited significantly poor survival times (Figure 2A; $p = 0.01$). Age, gender, T stage, tautological type, N stages, clinical stages, and the miRNA signature were used as covariates. Multivariate Cox regression analyses were used to investigate the independent prognostic value of the miR-602 signature (Table S1; $p < 0.01$).

To validate whether miR-602 expression is increased in ESCC, qRT-PCR was used to examine mature miR-602 levels in human ESCC tissues and normal esophageal tissues. We found that miR-602 levels in 108 ESCC tissues were markedly higher than those in normal esophageal tissues (Figure 2B; Table 1, validation group; $p < 0.05$), particularly in tissues with lymph node metastasis and advanced clinical stages of ESCC (Figures 2C and 2D; Table 1, validation group; $p < 0.05$). Kaplan-Meier survival analysis also revealed that miR-602 overexpression was associated with poor prognosis in patients with ESCC (Figure 2E; $p < 0.01$). The miRNA signatures were observed to be independent prognostic factors related to overall survival (OS) by multivariate Cox regression analysis (Table S1; $p < 0.01$).

Table 1. Correlation between miR-602 Expression and Clinicopathological Parameters of ESCC Patients

	Discovery Group (n = 93)			Validation Group (n = 108)		
Characteristic	Low (n = 19)	High (n = 74)	p Value	Low (n = 31)	High (n = 77)	p Value
Gender						
Male	15 (19.5%)	62 (80.5%)	0.618	24 (26.7%)	66 (73.3%)	0.295
Female	4 (25.0%)	12 (75.0%)		7 (38.9%)	11 (61.1%)	
Age (Years)						
≤60	6 (22.2%)	21 (77.8%)	0.784	8 (21.1%)	30 (78.9%)	0.195
>60	13 (19.7%)	53 (80.3%)		23 (32.9%)	47 (67.1%)	
Tumor Size (cm)						
<5	10 (19.6%)	41 (80.4%)	0.828	18 (25.7%)	52 (74.3%)	0.351
≥5	9 (21.4%)	33 (78.6%)		13 (34.2%)	25 (65.8%)	
Tumor Stage[a]						
T1 + T2	7 (31.8%)	15 (68.2%)	0.146	8 (30.8%)	18 (69.2%)	0.789
T3 + T4	11 (17.2%)	53 (82.8%)		23 (28.0%)	59 (72.0%)	
Histological Grade						
Well and moderate	16 (21.6%)	58 (78.4%)	0.574	24 (27.3%)	64 (72.7%)	0.490
Poor and NS	3 (15.8%)	16 (84.2%)		7 (35.0%)	13 (65.0%)	
Lymph Node Metastasis						
Negative	15 (33.3%)	30 (66.7%)	0.003	26 (43.3%)	34 (56.7%)	0.000
Positive	4 (8.3%)	44 (91.7%)		5 (10.4%)	43 (89.6%)	
Clinical Stage[a]						
I + II	15 (31.2%)	33 (68.8%)	0.006	25 (41.7%)	35 (58.3%)	0.001
III + IV	3 (7.5%)	37 (92.5%)		6 (12.5%)	43 (87.5%)	

[a]Numbers do not equal to the total number due to missing data.

Finally, we used the qRT-PCR method to assess the expression level of serum miR-602. The expression of the miRNA was significantly higher in ESCC patients than in the normal controls (Figure 2F; Table S2; $p < 0.01$). The results also revealed that serum miR-602 was positively associated with lymph node metastasis and advanced clinical stages of ESCC (Figures 2G and 2H; Table S2; $p < 0.01$). We then produced receiver operating characteristic (ROC) curves for ESCC diagnosis by serum miR-602, and we calculated the area under the curve, as well as the sensitivity and specificity of all thresholds. The area under the curve for plasma miR-602 was 0.895, indicating that there was a statistically significant difference in ESCC diagnosis by serum miR-602 marker (Figure 2I).

DNA Hypomethylation Results in miR-602 Overexpression in ESCC

The MassARRAY System allows quantitative high-throughput detection and analysis of a single CpG site methylation within a target fragment. A single CpG site or a combination of CpG sites forms a CpG unit. The miR-602 promoter is located in a typical CpG site, suggesting a possible involvement of DNA methylation in the regulation of miR-602 transcription (Figure S2). The amplicon detected in the promoter regions of miR-602 was 599 bp in length and contained 28 CpG sites that could be divided into 16 CpG units. The patterns observed in the cluster analysis indicated that the methylation status of miR-602 in ESCC tissues was notably different from that of normal esophageal cancer (Figure 3A). CpG methylation levels of the samples could be identified based on color for each miR-602 CpG unit in each sample. An obvious hierarchical clustering analysis was used to provide an equitable view of the relationships between ESCC and CpG units. We found that the densities of methylated CpG dinucleotides were higher in normal tissues than in ESCC tissues (Figure 3B).

Lastly, we assessed the methylation level of each CpG unit within the miR-602 promoter, and we found that 16 CpG units (except for CpG_1, CpG_3, and CpG_17) were more highly methylated in normal esophageal tissues than in ESCC tissues (Figure 3C; $p < 0.05$ or $p < 0.01$, respectively). Nonparametric test showed that, apart from CpG_1, CpG_3, and CpG_17, the mean methylation levels at CpG_2, CpG_4, CpG_5, CpG_6, CpG_7, CpG_8.9, CpG_10, CpG_11.12.13.14.15, CpG_16, CpG_18.19, CpG_20.21, CpG_22.23, CpG_24, CpG_25, CpG_26.27, and CpG_28 were all significantly higher in normal esophageal tissues (mean methylation = 92.22%, 93.83%, 41.72%, 76.11%, 75.00%, 80.11%, 48.22%, 95.33%, 96.06%, 80.72%, 97.61%, 94.06%, 95.67%, 86.67%, 90.17%, and 98.56%, respectively) than in ESCC (mean methylation = 43.50%, 49.89%, 29.28%, 35.94%, 47.17%, 41.83%, 35.33%, 35.33%, 42.28%, 51.22%,

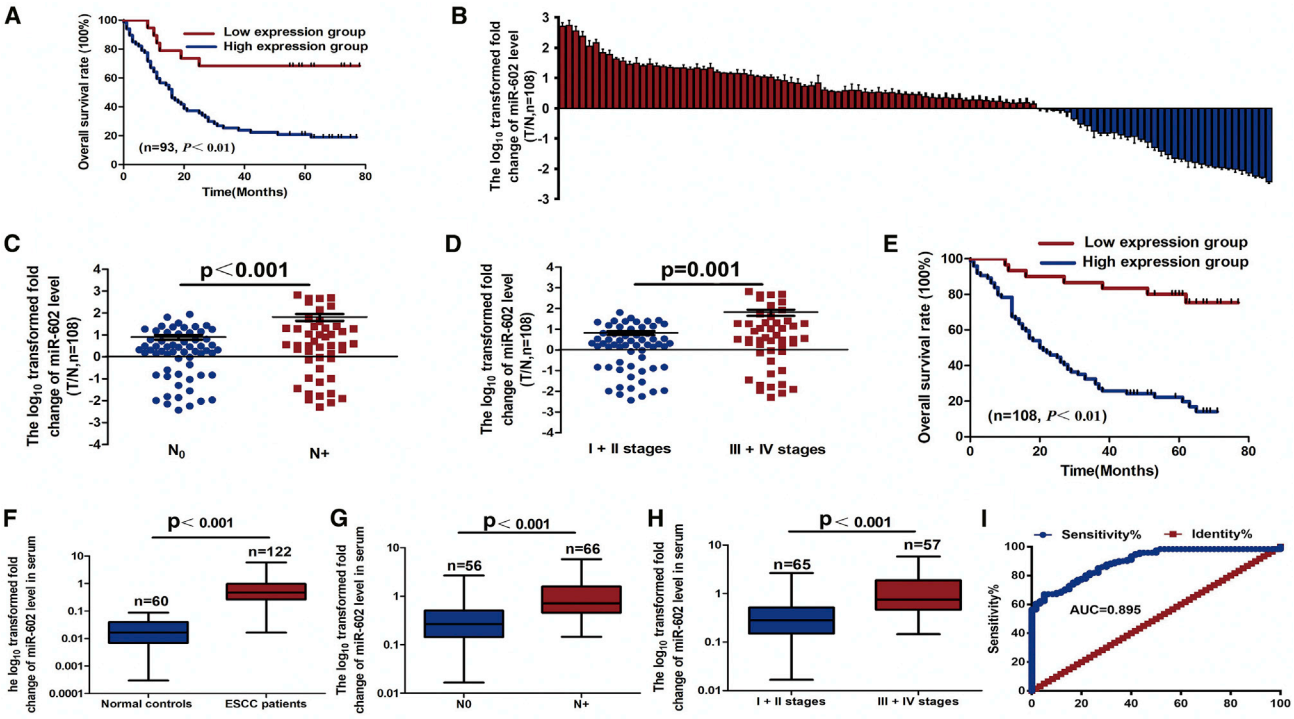

Figure 2. Relative miR-602 Expression Levels in ESCC Tissues and Serum and Their Clinical Significance

(A) Kaplan-Meier overall survival curves by high and low miR-602 expressions in 93 patient cases with ESCC. (B) Quantitation of miR-602 was performed using qRT-PCR in 108 paired ESCC (T) and corresponding normal tissues (N). The fold changes were calculated by relative quantification ($2^{-\Delta Ct}$, U6 as the internal control). (C and D) miR-602 expression was detected in lymph node metastasis (C) and different clinical stages (D) of ESCC. (E) Kaplan-Meier curves depicting overall survival according to the expression of miR-602 as validation. (F) The expression level of serum miR-602 in 122 ESCC patients and 60 healthy controls was measured by qRT-PCR and normalized to U6. (G and H) miR-602 expression was detected in lymph node metastasis (G) and different clinical stages (H). (I) Receiver operating characteristic (ROC) curve analysis of the miR-602 assay ratio for detecting ESCC patients.

41.22%, 42.17%, 40.00%, and 51.56%, $p < 0.05$ or $p < 0.01$, respectively).

For the purpose of the result, 5-aza-2′-deoxycytidine (5-aza-CdR), the demethylation agent, was used to reverse methylation. The methylation level of miR-602 was obviously inactivated in KYSE150 (81.59%) and KYSE450 (85.52%) cell lines compared with two corresponding untreated cell lines (22.11% and 18.89%, respectively), with the downregulation of methylation status treated with 5-aza-CdR (Figure 3D; $p < 0.01$). Correspondingly, there were higher expression levels of miR-602 in KYSE150 and KYSE450 cells treated with 5-aza-CdR compared to two untreated cell lines, which were negatively correlated with methylation status in ESCC cell lines (Figure 3E; $p < 0.01$). This showed direct evidence that the overexpression of miR-602 in the ESCC tissues was correlated with promoter hypomethylation and demethylation of the promoter genes could upregulate the expression of miR-602.

miR-602 Showed Positive Effects on ESCC Cell Growth and Metastasis

Owing to their lower expression of miR-602 among seven ESCC cell lines (Figure 4A), the KYSE150 and KYSE450 cell lines were selected in a later overexpression study. To further investigate the role of miR-602 in the regulation of ESCC cell proliferation, colony formation, invasion, and migration, KYSE150 and KYSE450 cells were transfected with a miR-602 mimic, and miR-602 levels were then examined using qRT-PCR. The efficiency of transfection was verified by a significant increase in miR-602 expression in KYSE150 and KYSE450 cells, which was determined by qRT-PCR (Figure 4B; $p < 0.01$). We found that high exogenous expression of miR-602 remarkably promoted proliferation, colony formation, migration, and invasion of KYSE150 and KYSE450 cells (Figures 4C–4H; $p < 0.05$ or $p < 0.01$). We further observed that forced expression of miR-602 could decrease the number of cells in G1 phase and increase the numbers of cells in S and M phases (Figures 4I and 4J).

Next, we transfected ESCC cells with inhibitors of miR-602 to confirm the opposite results of mimic transfection (Figure S3A; $p < 0.01$). As expected, downregulation of miR-602 using the inhibitors could decrease the malignant phenotype of KYSE180 and KYSE510 cells *in vitro*, including cell growth (Figures S3B and S3C; $p < 0.01$), colony formation (Figures S3D and S3E; $p < 0.01$), as well as cell migration and invasion (Figures S3F and S3G; $p < 0.05$

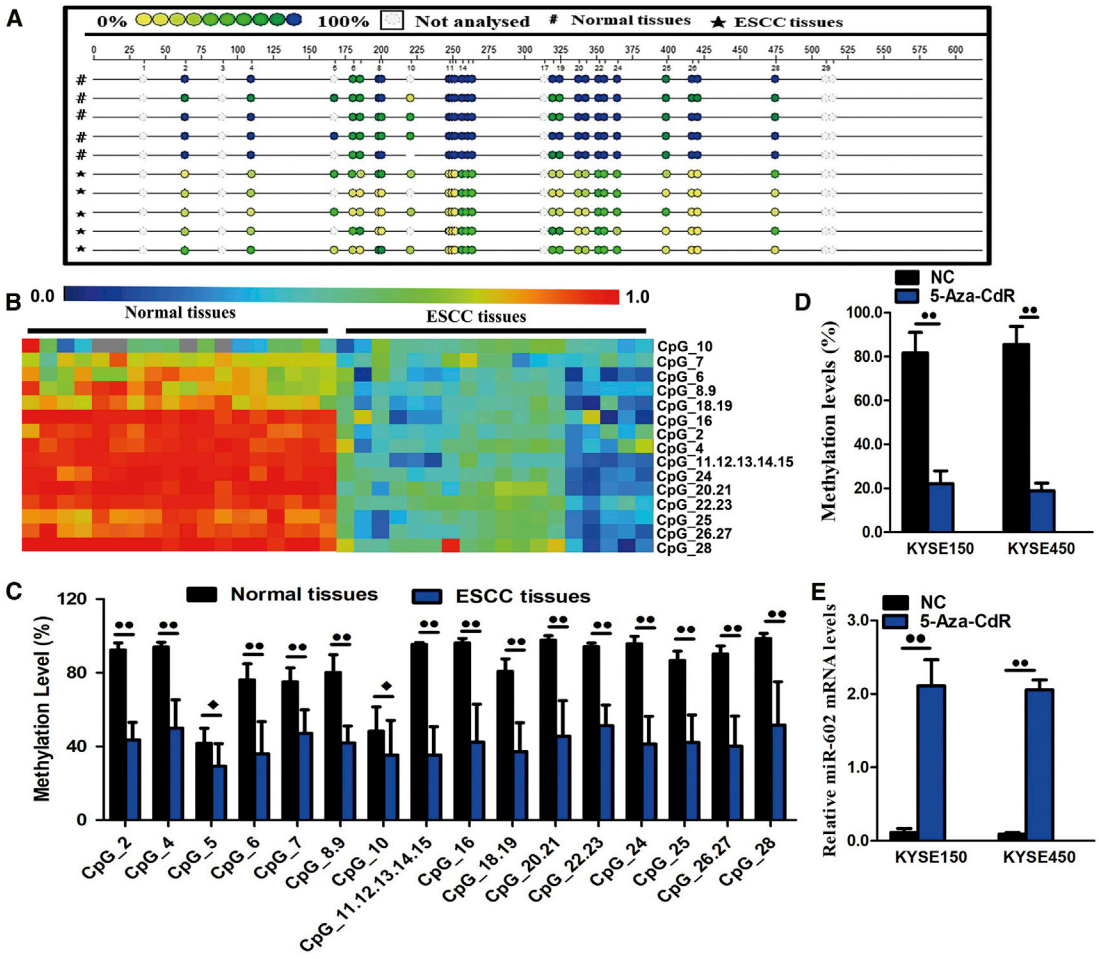

Figure 3. DNA Methylation Status of the miR-602

(A) Methylation profile of CpG sites for the miR-602 gene. The color of the circles is related to the percentage of methylation in each CpG site. Boxes indicate the different methylation patterns between 18 ESCC samples and corresponding normal tissues. (B) Hierarchical cluster analysis of CpG sites' methylation profiles of miR-602 promoter region in esophageal squamous cell carcinoma (n = 18) and normal esophageal tumors (n = 18). The color gradient between blue and red indicates methylation of each miR-602 unit in each sample ranging from 0% to 100%. Gray represents technically inadequate or missing data. (C) Evaluation of CpG methylation within the miR-602 promoter. The distribution of 16 analyzed CpG units within miR-602 is shown. (D) DNA methylation levels of the miR-602 promoter region in 5-aza-CdR-treated KYSE150 and KYSE450 cells by BSP assay. (E) Quantitation of the miR-602 level after treatment with 5-aza-CdR in KYSE150 and KYSE450 cell lines. Data are presented as the mean value ± SD from triplicate experiments. ●$p < 0.05$, ●●$p < 0.01$, ■■■$p > 0.05$.

or $p < 0.01$). Moreover, upon the downregulation of miR-602, the cell G1 percentages of KYSE180 and KYSE510 cells clearly increased compared with the percentages measured in controls (Figures S3H and S3I; $p < 0.05$), indicating that miR-602 downexpression resulted in cycle conversion in ESCC cells.

miR-602 Targets FOXK2 to Contribute Proliferation and Metastasis

To explore the mechanism through which miR-602 regulates ESCC cell progression, we searched for potential downstream regulatory targets of miR-602 using several bioinformatics methods, including miRDB, miRTarBase, TargetScan, and miRWalk (Figure 5A). Then, several candidate genes involved in proliferation, cell cycle, and invasion-metastasis were detected by gene ontology (GO) terms and qRT-PCR. We found that the 3′ UTR of Fork head box (FOX) K2 (FOXK2) mRNA contains sequences that are complementary to being potential targets of miR-602 (Figure 5B; $p < 0.01$).

To verify whether FOXK2 was a direct target of miR-602, we transfected KYSE150 and KYSE450 cells with miR-602 mimic, and we found it could remarkably downregulate the mRNA and protein levels of FOXK2, respectively (Figure 5C; $p < 0.01$). We also transfected KYSE180 and KYSE510 cells with inhibitors of miR-602 to confirm the results of mimic transfection. As expected, downregulation of miR-602 using inhibitors could enhance the FOXK2 mRNA and protein levels in KYSE150 and KYSE510 cells (Figure 5D; $p < 0.01$).

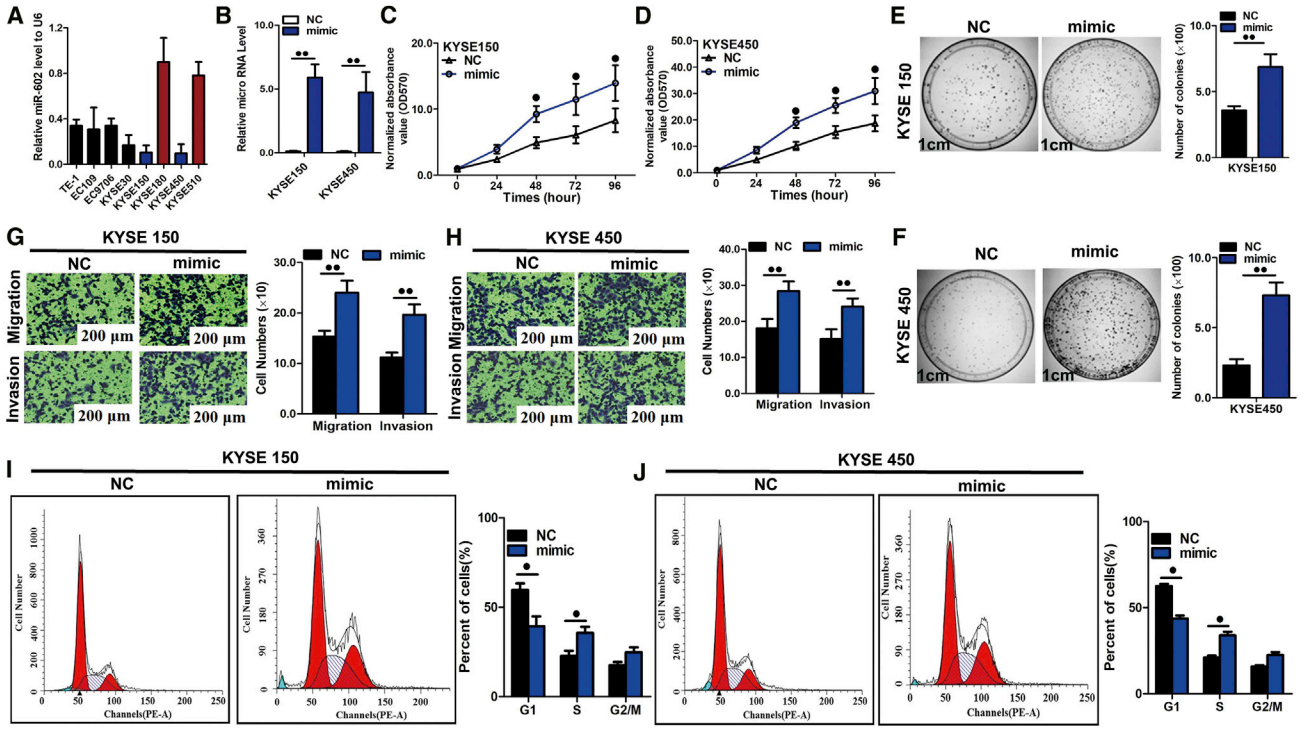

Figure 4. miR-602 Overexpression Regulated Cell Proliferation, Metastasis, and Cell Cycles

(A) RNA level of miR-602 in 7 ESCC cell lines. (B) Quantitation of the miR-602 level after transfection of miR-602 mimic in KYSE150 and KYSE450 cell lines. (C and D) The cell growth curve was measured by MTS after transfection of the miR-602 mimic in KYSE150 (C) and KYSE450 (D) cell lines, and the OD 570 was normalized to the star point (0 h). (E and F) Representative images and quantitation of colony formation were performed after transfection of miR-602 mimic in KYSE150 (E) and KYSE450 (F) cell lines. (G and H) Representative images and quantitation of the transwell assay were performed after transfection of the miR-602 mimic in KYSE150 (G) and KYSE450 (H) cell lines. (I and J) miR-602 induced cell-cycle arrest at the G1/S phase in KYSE150 (I) and KYSE450 (J) cell lines. Data are presented as the mean value ± SD from triplicate experiments. $^{\bullet}p < 0.05$, $^{\bullet\bullet}p < 0.01$.

We next applied the dual-luciferase reporter assay to reveal the regulation of miR-602 by FOXK2. The fragments containing the miR-602-binding sequence or -mutated sequence in the 3′ UTR regions of FOXK2 were cloned into the pmiR-RB-REPORT vector luciferase reporter. These reporter constructs were co-transfected with miR-602 mimic or miR-negative control (NC) into KYSE150 and KYSE450 cells, and the luciferase activities were subsequently measured. The miR-602 mimic significantly suppressed the luciferase activity of pmiR-RB-REPORT-FOXK2-3′ UTR (Figure 5E; $p < 0.01$), while miR-NC had no inhibitory effect on pmiR-RB-REPORT-FOXK2-3′ UTR. The miR-602 inhibition of pmiR-RB-REPORT-FOXK2-3′ UTR was sequence specific because the luciferase activities of pmiR-RB-REPORT-FOXK2-MUT did not decrease in the presence of miR-602. Taken together, the results suggest that miR-602 can directly target the 3′ UTR of miR-602.

A rescue experiment was performed to confirm that FOXK2 was the functional target of miR-602 in KYSE150 cells. The evidence was obtained from the observation that the FOXK2 mRNA and proteins (endogenous) in ESCC cell were abolished by mimic transfection and recovered by transfection of both pEGFP-N1-FOXK2 expression constructs, respectively (Figures 6A and 6B; $p < 0.01$). The results showed that migration and invasion created by mimic transfection were reversed by the transfection of both expression constructs (Figure 6C; $p < 0.05$ or $p < 0.01$). Furthermore, the expression of FOXK2 was silenced by small interfering RNA (siRNA) transfection in KYSE150 cells, which showed that its expression was significantly attenuated at the mRNA and protein levels (Figure 6D; $p < 0.01$). Post-FOXK2 silencing, migration and invasion abilities were significantly increased (Figure 6E; $p < 0.05$ and $p < 0.01$). These results further prove that FOXK2 may be a downstream target of miR-602.

miR-602 Accelerates Tumor Growth and Metastasis *In Vivo*

Finally, we evaluated the effects of miR-602 on the growth and metastasis of ESCC in nude mice. KYSE450 cells were transfected with either a lentiviral expression vector to increase miR-602 (Lenti-mimic) or a NC lentiviral vector (Lenti-vector). Efficient overexpression of miR-602 in the KYSE450 cells following lentiviral infection was verified by qRT-PCR (Figure 7A; $p < 0.01$). Then, we injected these KYSE450 cells into mice subcutaneously to build transplanted tumors in 6 BALB/c nude mice. Beginning on day 7 after implantation, the tumor lengths and widths were measured every 5 days to produce 6 measurements. The tumor growth curve revealed a significant acceleration in the miR-602-overexpressing group compared

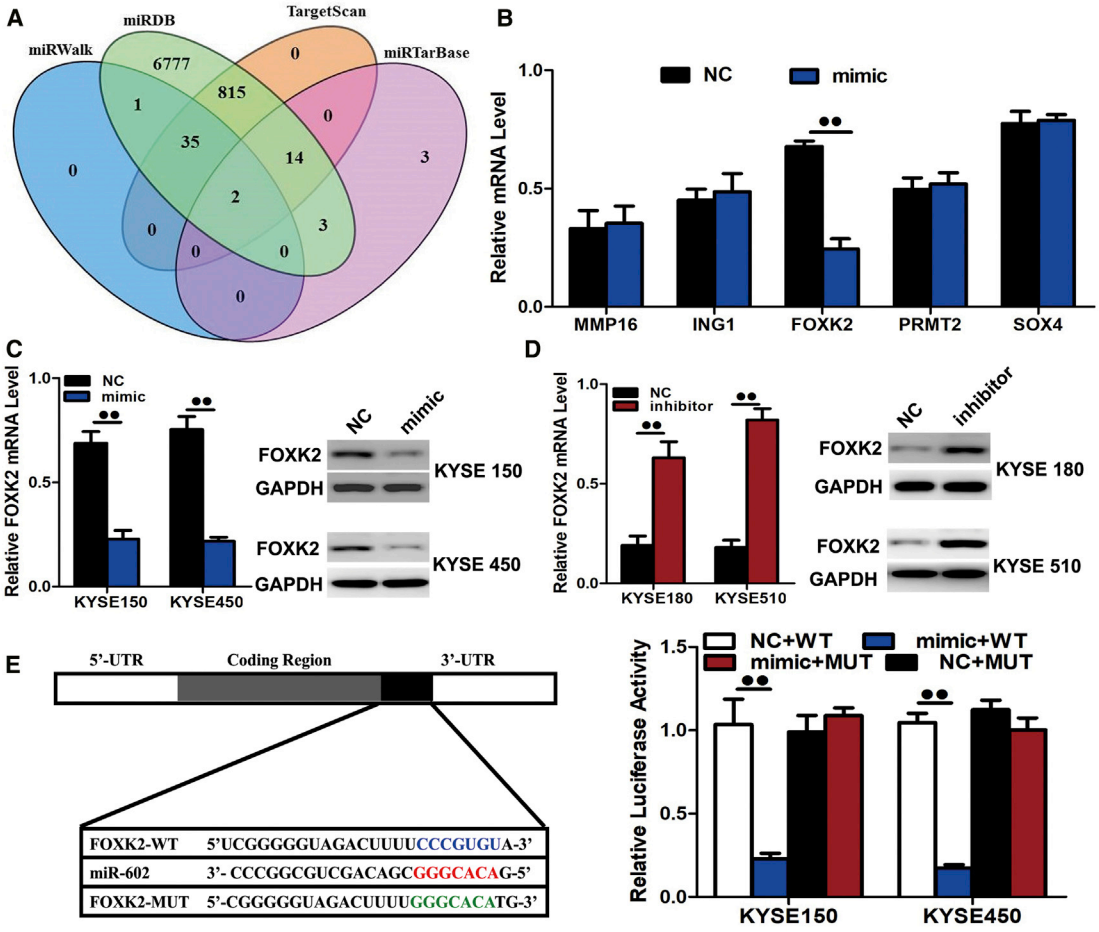

Figure 5. FOXK2 Was One Direct Target Gene of miR-602

(A and B) FOXK2 was identified as a potential regulatory target of miR-602 by considering the downregulation of genes using prediction tools (A) and qRT-PCR (B). (C) The expression levels of FOXK2 mRNA and protein were measured by qRT-PCR and western blot analysis using GAPDH as the loading control, after transfection of miR-602 mimic in the KYSE150 and KYSE450 cell lines, respectively. (D) The expression levels of FOXK2 mRNA and protein were measured by qRT-PCR and western blot analysis using GAPDH as the loading control, after transfection of miR-602 inhibitors in the KYSE180 and KYSE510 cell lines, respectively. (E) Dual-luciferase reporter assay. The relative luciferase activity was normalized to the Renilla luciferase activity assay after co-transfection of cells with miR-602 mimic and miR-RB-REPORT constructs containing the wild-type (WT) or mutant (MUT) FOXK2 3′ UTR region in KYSE180 and KYSE510 cell lines. Data are presented as the mean value ± SD from triplicate experiments. $^{\bullet}p < 0.05$, $^{\bullet\bullet}p < 0.01$.

with the control group (Figure 7B; $p < 0.05$ or $p < 0.01$). Subsequently, the tumors were dissected, and the exact sizes and weights were evaluated. Compared with those of the control group, the mean volume and mass of the tumors in the miR-602-overexpressing group were significantly larger and heavier (Figures 7C and 7D; $p < 0.01$).

In the tail vein of 6 nude mice, 10^6 luciferase-labeled cells were injected intravenously for 6 weeks. Luciferase activity was used to evaluate tumor burden in nude mice. The lung, liver, bone, and adrenal gland metastases were significantly higher in the mice injected with cells featuring the miR-602-overexpressing group compared with those in the control group (Figures 7E and 7F). All these results obtained for the mouse models suggest that miR-602 plays important roles in ESCC growth and metastasis.

To determine whether miR-602 antagomir could inhibit the growth of ESCC in nude mice, we established a BALB/c nude mouse tumorigenic model using KYSE180 cells. After 7 days, miR-602 antagomir or miR antagomir NC was directly injected into the implanted tumor every 5 days. The tumor volume was measured every 5 days until day 42. The tumor volume and weight of mice treated with miR-602 antagomir were significantly lower than those of mice treated with miR antagomir NC (Figures 7G–7I; $p < 0.01$). This result indicated that miR-602 has the therapeutic characteristics in ESCC cells of the nude mouse model.

Additionally, the proliferative activities of the tumor cells were assessed by immunohistochemical staining for Ki67 in formalin-fixed paraffin-embedded (FFPE) tissues of xenograft tumors. The Ki67 staining intensities were decreased in tumors from the miR-602 antagomir group

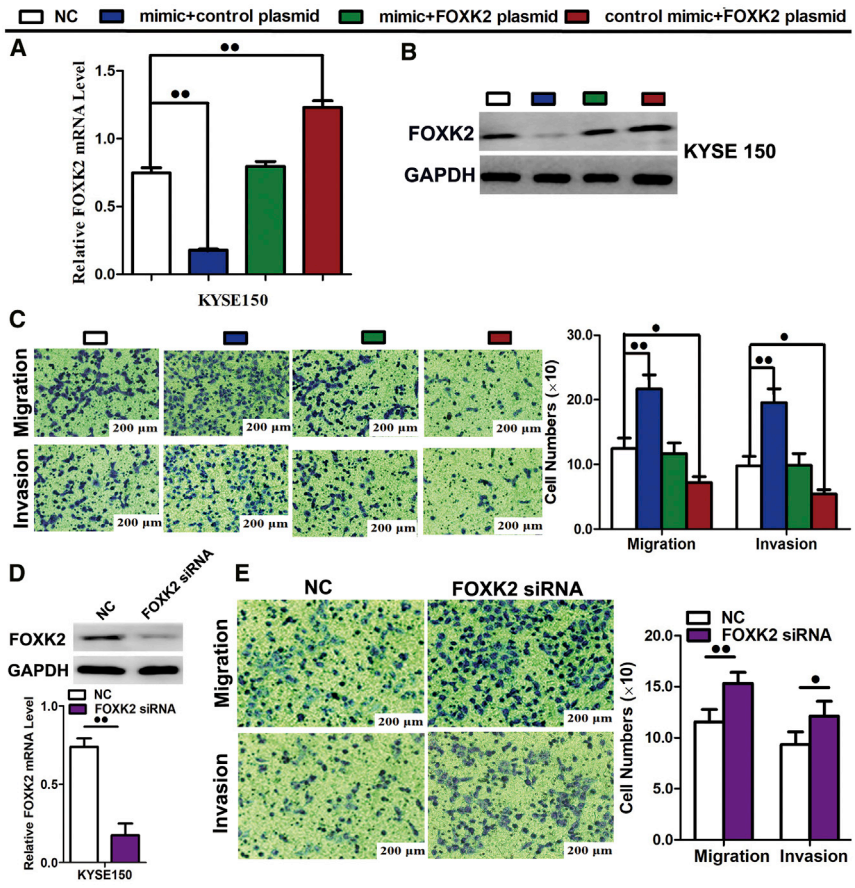

Figure 6. A Rescue Assay Was Further Performed to Confirm that FOXK2 Was the Functional Target of miR-602

(A and B) The mRNA (A) and protein (B) levels of FOXK2 in KYSE150 cell lines co-transfected with miR-602 mimic and pEGFP-C1 plasmid containing the FOXK2 CDS sequence. (C) Transwell assay of cells co-transfected with miR-602 mimic and FOXK2 plasmids. (D) The expression of FOXK2 at the mRNA and protein levels after siRNA silencing in KYSE150 cells. (E) Representative images and quantification of transwell assay after the transfection of FOXK2 siRNA into the KYSE150 cell lines. Data are presented as the mean value ± SD from triplicate experiments. $^{\bullet}p < 0.05$, $^{\bullet\bullet}p < 0.01$.

(Figure 7J). Moreover, a distinct increase in FOXK2 expression was observed in xenograft tumors of the miR-602 antagomir group compared with the expression observed for the miR antagomir NC group (Figure 7J). In an analysis of 80 paired tumor and adjacent non-tumor tissue samples, we found that FOXK2 expression was significantly lower in tumor tissues than in adjacent non-tumor tissues (Figure 7K; Table S3). We also conducted a Spearman correlation coefficient analysis to determine the association of miR-602 expression level and FOXK2 expression in 80 ESCC tissue samples. miR-602 expression levels were inversely correlated with the downregulation levels of FOXK2 in the 80 ESCC specimens (Figure 7L; $p < 0.05$).

DISCUSSION

Accumulating evidence has shown that miRNAs could function as critical modulators in tumorigenesis, having emerged as tumor oncogenes and suppressors by different target genes.[19,20] Specific miRNAs in blood or tissue samples could serve as novel biomarkers, and detection of these could contribute to cancer diagnosis and clinical outcome prediction.[21–23] In the current research, we analyzed the expression of miR-602 in ESCC tumors compared with that in the corresponding non-cancerous esophageal tissues. It is the first time to identify miR-602 expression in ESCC. We found that miR-602 was significantly upregulated in ESCC compared with corresponding normal tissue, and it increased along with ESCC progression and was an independent risk prognostic factor for ESCC patients. Importantly, we first detected a high expression of miR-602 in preoperative ESCC serum, and the miR-602 levels in serum and tissues were associated with lymph node metastasis and TNM stages. These results implied that miR-602 may act as a tumor oncogene, which might provide a possibility to predict ESCC progression.

In fact, accumulating reports have suggested that the presence of tumors tissues and circulating miRNAs and their potential use as novel biomarkers for cancers. The reduced expressions of miRNAs such as miR-138 and miR-145 have been noted in ESCC tissues.[24,25] Conversely, miR-21, miR-200c, and miR-133a have been reported to be upregulated in esophageal cancer.[26,27] Moreover, concerning ESCC, there have been three reports on the role of circulating miRNAs in the plasma or serum of patients with ESCC.[28–30] The serum-based approach is more advantageous than biopsy, an invasive procedure that serves as the main tool for ESCC risk assessment.[31] Therefore, to the best of our knowledge, our study is the first to report the diagnostic and prognostic values of tissue and serum miR-602.

It is well known that miRNAs usually function as oncogenes or tumor suppressors to control many cellular events in tumor development and progression.[31] Similar to tumor suppressors, dysregulation of tumor suppressor-type miRNAs by epigenetic silencing is often observed in human cancers, such as miR-142-3p, miR-142-3p, and miR-183.[32–34] We supposed that the upregulated miR-602 was epigenetically activated by DNA hypomethylation. Correspondingly, CpG site hypomethylation of miR-602 was observed in ESCC clinical samples, and this further verified that hypomethylation by 5-aza-CdR could dramatically augment the expression of miR-602 in ESCC cell lines. These data support not only the notion that DNA hypomethylation epigenetic amplification of miR-602 but also epigenetic amplification of miR-602 actively occur during the tumor

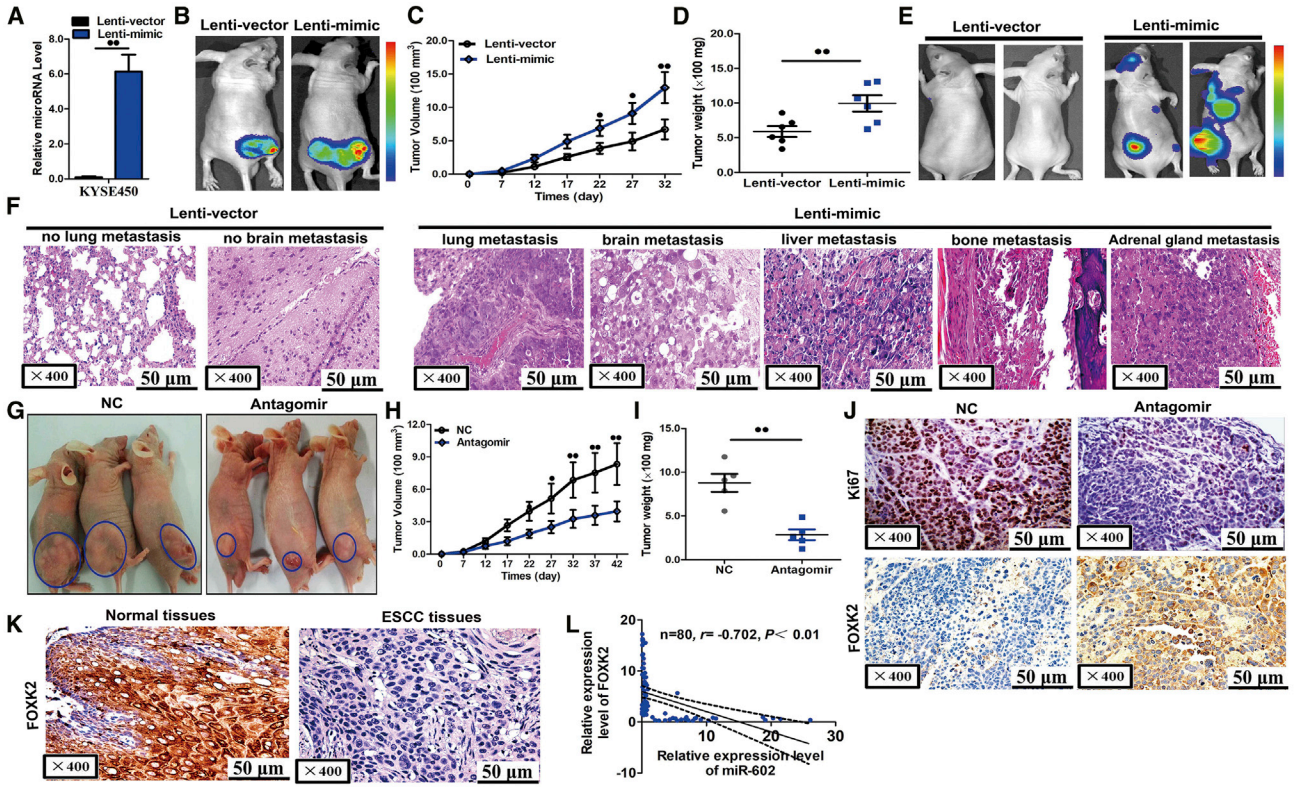

Figure 7. miR-602 Hampered Tumor Growth and Metastasis *In Vivo*

(A) Levels of miR-602 in stable overexpressing KYSE450 cells (Lenti-mimic) and control cells (Lenti-vector). (B–D) Stable miR-602-overexpressing KYSE450 cells were subcutaneously injected into nude mice to form solid tumors (B), and representative images of tumor volumes (C) and weights (D) were analyzed by *in vivo* luciferase imaging on the last day of analysis (n = 6 for each group). (E and F) The metastatic nodules (E) were observed in the lungs, brains, liver, bone, and adrenal gland of mice (F) treated with stable miR-602-overexpressing KYSE450 cells or control vector cells by the vein injection method. (G–I) KYSE180 cells were subcutaneously injected into nude mice to form solid tumors (G) and synchronously treated with miR-602 antagomir or miR antagomir NC (n = 5 for each group). A 10-nmol miR-602 antagomir as well as the miRNA negative control in 0.1 mL saline buffer was locally injected into nude mice to treat tumor mass once every 5 days for 6 weeks. Tumor volume (H) and weight (I) in nude mice are quantified. (J) Immunohistochemical staining of Ki67 and FOXK2 in tumor tissues dissected from nude mice treated with miR-602 antagomir or miR antagomir NC. (K) FOXK2 protein expression measured by immunohistochemical staining in 80 ESCC samples and pair-matched esophageal tissues. (L) Spearman correlation analysis of the negative correlation between the expression of miR-602 and FOXK2. $^{\bullet}p < 0.05$, $^{\bullet\bullet}p < 0.01$.

development and progression of ESCC cancer.[35–37] This is the first study to reveal that the potential molecular alterations by DNA methylation regulate miR-602 status.

To date, there have been no studies of the biological functions of miR-602 in ESCC. We further investigated the function of miR-602 in four representative cell lines: KYSE150, KYSE180, KYSE450, and KYSE510 cells. We transfected mimics or inhibitor into cells, thus increasing or decreasing the miR-602 level. An increase in miR-602 was found to promote the proliferation, migration, and invasion of KYSE150 and KYSE450 cells, while decreased miR-602 expression inhibited the proliferation, migration, and invasion of tumor cells. We further conducted fluorescence-activated cell sorting analysis to confirm the role of miR-602 as a negative regulator of the cell cycle, and we found that increased expression of this miRNA resulted in significant G0/G1 reduction and S and M phase arrest.

Distant metastasis is the major reason for treatment failure in ESCC, and, thus, early diagnosis and early treatment for metastasis are critical to improve the outcomes. In this study, we have demonstrated the high expression of miR-602 in metastatic ESCC specimens in contrast to non-progression ESCC or non-cancerous esophageal tissues. Moreover, increased miR-602 expression induced tumor formation and metastasis in nude mice. More importantly, the administration of miR-602 has significant efficacy in suppressing the growth of transplantation tumor *in vivo*, suggesting miR-602 as a potential therapeutic target for ESCC. These results indicated that miR-602 plays a crucial role in the growth and metastasis of ESCC. Therefore, therapies targeting miR-602, combined with existing conventional antitumor therapies, may serve as an effective treatment approach for ESCC patients with high metastatic risk. Understanding the underlying mechanisms responsible for miR-602-related metastasis may reveal additional strategies for miR-602 intervention.

The specific mechanism of miR-602 involved in ESCC is still unknown. To elucidate the underlying mechanism, we searched four miRNA databases. We first identified FOXK2 as one of the direct and functional targets for miR-602 based on several lines of evidence. First, miR-602 directly bound to seed-complementary binding sites in the 3′ UTR of FOXK2 mRNA and repressed upstream luciferase activity. Point mutations of several nucleotides in binding sites were adequate to abolish the effect of miR-602. Second, the expressions of miR-602 and FOXK2 were inversely correlated in xenograft tumors and human ESCC tissue samples. Third, up- and downregulation of miR-602 decreased and increased FOXK2, respectively. Last and more importantly, decreased FOXK2 expression largely accelerated the biological function mediated by the forced expression of miR-602.

FOXK2 is a member of the FOX transcription factor family.[38] Recent researchers discovered that overexpression of FOXK2 inhibits the proliferation and metastasis of breast cancer, lung cancer, and hepatocellular cancer and is related to the clinical prognosis.[38–40] FOXK2 is involved in several signaling pathways, such as the mammalian target of rapamycin-, WNT-, AKT-, and EMT-signaling pathways. These signaling pathways regulate cell proliferation and death by influencing the expression of important genes through the transcription repressor FOXK2.[41–43] The ability of FOXK2 overexpression to retard the invasion effects of miR-602 clearly indicates the importance of their relationship in ESCC metastasis. FOXK2 levels correlated with lymph node metastasis ratio and advanced clinical stages. These results were also consistent with a previous report that suggested that lower FOXK2 expression significantly induced the migration of other cancer cell types.[38–43]

In summary, our study reported, for the first time, that increased expression of miR-602 caused by its promoter hypomethylation is functionally associated with the potency of growth and metastasis in ESCC by regulating FOXK2. Moreover, serum miR-602 might provide a novel and stable marker and act as an independent predictor of OS for patients with ESCC. Our findings suggest that miR-602 functions as a tumor oncogene in ESCC and holds promise as a prognostic biomarker and potential therapeutic target for ESCC.

MATERIALS AND METHODS

Tissue Samples and Ethics Statement

An organized chip array including 93 cases of ESCC tissues and non-neoplastic esophageal tissues was purchased from Outdo Biotech (HEso-Squ180Sur-02 and HEso-Squ180Sur-03, Shanghai, China; http://www.superchip.com.cn/). Another 108 paired frozen paraffin ESCC tissues and matched adjacent non-cancerous tissues were obtained from North China University of Science and Technology Affiliated People's Hospital, from 2009 to 2013. Serum samples from 122 ESCC patients and 60 healthy controls were obtained from the above-mentioned hospital. All serum specimens were transported at 4°C and stored at −80°C until RNA extraction. This study was carried out after approval by the ethics committee of the hospital and after obtaining informed consent from all subjects. All patient samples were obtained with full written consent, and all samples were collected from tissues that remained after the completion of diagnosis from pathology.

Cell Lines and Cell Culture

Human ESCC cell lines TE-1, EC-109, KYSE-30, KYSE-150, KYSE-180, KYSE-450, and KYSE-510 were obtained from the Cell Culture Center of Peking Union Medical College (Beijing, China) and Typical Culture Cell Bank of Chinese Academy of Sciences (Shanghai, China). The HEK293T cells were obtained from ATCC (Manassas, VA). Human ESCC cell lines were cultured in RPMI-1640 medium, and HEK293T cells were maintained in DMEM supplemented with 10% fetal bovine serum (Gibco BRL, Grand Island, NY) in a humidified atmosphere of 5% CO_2 at 37°C.

In Situ Hybridization of miR-602

In situ hybridization (ISH) was performed according to the manufacturer's instructions (Roche, Pleasanton, CA, USA). The miR-602 (5′-CAGCTGTCGCCCGTGTC-3′) was tagged with 3′ and 5′ digoxigenin (http://redlandbio.biomart.cn/, Guangzhou, China). U6 small nuclear RNA (snRNA) (5′-CACGAATTTGCGTGTCATCCTT-3′) and scrambled probes (5′-GTGTAACACGTCTATACGCCCA-3′) were used as positive and NCs, respectively. The probe-target complex was detected using an antidigoxigenin-alkaline phosphate conjugate and nitro-blue tetrazolium and 5-bromo-4-chloro-3′-indolyphosphate as the chromogen. The blue color of staining was defined as positive expression of miR-602 by using *in situ* hybridization. All the images were observed and diagnosed by two clinical pathologists independently. At least five random fields in one sample were scanned and evaluated by pathologists blinded to grouping and clinical features. The stainings were classified as follows: (1) low expression, the positive cells <50%; and (2) high expression, the positive cells ≥50%.

DNA Extraction and Bisulfite Modification

Genome DNA was prepared from ESCC cell lines and 18 paired frozen fresh ESCC tissues and matched adjacent non-cancerous tissues. Purified genomic bisulfite-converted DNA samples were also successfully tested by PCR with human miR-602 primers 5′-aggaagagGTTTTAGTGAGAGTTGGGGGAGA-3′ (forward) and 5′-cagtaatacgactcactatagggagaaggctCTAAATAAAACCCTAAAATCCCCAA-3′(reverse) to show that the samples could be used for follow-up experiments. A NanoDrop 2000 spectrophotometer was used to measure the converted DNA (Thermo Fisher Scientific). Then, transformed DNA was PCR amplified using the TaKaRa rTaq Kit (R001B, TaKaRa, Dalian, China).

Quantitative Analysis of DNA Methylation

The University of California, Santa Cruz (UCSC) Genome Browser (http://genome.ucsc.edu) was used to identify the sequence of the CpG sites. Primer sets for the methylation analysis of the miR-602 promoter were designed using EpiDesigner (http://www.epidesigner.com/start.html). For each reverse primer, an additional T7 promoter tag was added for *in vivo* transcription, and a 10-mer tag was added to the forward primer to adjust for the melting

temperature. Methylation of miR-602 was quantitatively analyzed by the MassARRAY platform (Agena Bioscience). MALDI-TOF mass spectrometry (MS), a new type of high-throughput quantitative methylation detection method, was combined with the base specificity of the enzyme reaction to test the methylation level of DNA. Mass spectra were collected by MassARRAY Compact MALDI-TOF (Agena Bioscience), and the methylation proportions of individual units were generated by EpiTyper 1.0.5 (Agena Bioscience). Non-applicable readings and their corresponding sites were eliminated from analysis. Methylation level was expressed as the percentage of methylated cytosines over the total number of methylated and unmethylated cytosines.

Cell Line Treatment with Epigenetic-Modulating Drug

5-Aza-20-deoxycytidine treatment of the ESCC cell lines were treated with 1.5 mmol/L 5-aza-20-deoxycytidine (Sigma A3656) for 96 h. At 24 h before harvest, 0.5 mmol/L Trichostatin A (Sigma T8552) was added. DNA, RNA, and protein were extracted and analyzed for the methylation status of the miR-602 promoter, as well as expression of miR-602 and its targeted proteins.

miRNA Transfection

All endogenous mature miRNA mimics, inhibitors, and agomirs were purchased from RiboBio (Guangzhou, China). For transfection, experimental protocols were performed according to the manufacturer's protocols. miRNA mimics, miRNA inhibitors, and miRNA NC were transfected into cells using Lipofectamine 2000 (Invitrogen, Carlsbad, USA), according to the manufacturer's instructions. After 48 h of transfection, cells were used for further experiments.

siRNA Knockdown

The siRNA for FOXK2 (5′-GUUAUCAGUCUGAGCCAGG-3′) was synthesized by RiboBio (Guangzhou, China). siRNA was transfected individually into cells at the indicated concentrations using Lipofectamine RNAiMAX (Invitrogen), according to the manufacturer's instructions. For concurrent inhibition of a target gene, mixtures of siRNAs (in total 70 nmol/L of each 10 nmol/L) or nonspecific control siRNAs (in 70 nmol/L) were transfected into ESCC cells, respectively.

Plasmid Construction

pDonR223-FOXK2 plasmids carrying the human FOXK2 gene were purchased from Changsha Axybio Bio-Tech (Changsha, China). The complete coding sequences of human FOXK2 were amplified from pDonR223-FOXK2 plasmids. FOXK2 products and pEGFP-N1 plasmid were digested with Xho I and Hind III; fragments were purified and ligated with T4 DNA ligase. The ligated product was transformed into TOP10-competent cells, and the positive clone was named pEGFP-N1-FOXK2.

Quantitative Real-Time PCR

Total miRNA was extracted from frozen tissues or cultured cells using TRIzol total RNA isolation reagent (Invitrogen), according to the manufacturer's instructions. cDNA was synthesized from total RNA or purified small RNAs using gene-specific primers or random hexamers with the SUPERSCRIPT III Reverse Transcriptase Kit (Invitrogen), according to the manufacturer's instructions. miRNAs were detected with stem-loop primers purchased from RiboBio as described (Guangzhou RiboBio). GAPDH and U6 small nucleolar RNA were used for normalization. qPCR was conducted using a QuantiTect SYBR Green PCR Kit (TaKaRa Bio, Japan) on a StepOne Real-Time PCR System (Applied Biosystems, CA). Relative expression levels were calculated using the $2^{-\Delta\Delta Ct}$ method (Bio-Rad CFX manager software 3.1). To evaluate the expression of FOXK2, total RNAs were used for the RT reactions, and qPCR) was performed on a Step One Plus real-time system (Applied Biosystems, Carlsbad, CA). All the primers used in this research are listed in Table S4.

Target Prediction and Luciferase Reporter Assays

Bioinformatics analysis was performed using the following programs: miRWalk, miRDB, and miRTarBase. The 3′ UTR of human FOXK2 was amplified from human genomic DNA and individually inserted into the pmiR-RB-REPORT (Ribobio, Guangzhou, China) using the XhoI and NotI sites. Similarly, the fragment of FOXK2 3′ UTR mutant was inserted into the pmiR-RB-REPORT control vector at the same sites. For reporter assays, ESCC cells were co-transfected with wild-type reporter plasmid and miR-602 mimic. Firefly and Renilla luciferase activities were measured in cell lysates using the Dual-Luciferase Reporter Assay system. Luciferase activity was measured 48 h post-transfection using the dual-glo luciferase reporter system, according to the manufacturer's instructions. Firefly luciferase units were normalized against Renilla luciferase units to control for transfection efficiency.

In Vitro Cell Proliferation Assays

For cell proliferation assays, cells were seeded into each well of a 96-well plate (5×10^3/well), and the cell proliferation ability was determined by MTS (3-(4,5-dimethylthiazol-2-yl)-5-(3-carboxymethoxyphenyl)-2-(4-sulfophenyl)-2H-tetrazolium), according to the manufacturer's instructions. MTS solution was added (20 μL/well) to each well and incubated at 37°C for 2 h. The optical density of each sample was immediately measured using a microplate reader (Bio-Rad, Hercules, CA, USA) at 570 nm.

Colony Formation Assay

ESCC cells were transfected with miR-602 mimic, miR mimic NC, miR-602 inhibitor, or miR inhibitor NC. Then 24 h later, transfected cells were trypsinized, counted, and replated at a density of 1×10^3 cells/10-cm dish. Then 10 days later, colonies resulting from the surviving cells were fixed with 3.7% methanol, stained with 0.1% crystal violet, and counted. Colonies containing at least 50 cells were scored. Each assay was performed in triplicate.

Transwell Migration and Invasion Assay

In vitro cell migration assays were performed as per the manufacturer's instructions using transwell chambers (8 μM pore size; Costar). Cells were allowed to grow to subconfluency (~75%–80%) and were serum starved for 24 h. After detachment with trypsin, cells were washed with PBS and resuspended in serum-free medium. Next,

a 100 μL cell suspension (5×10^4 cells/mL) was added to the upper chamber. Complete medium was added to the bottom wells of the chambers. For the screen, the cells that had not migrated after 24 h were removed from the upper face of the filters using cotton swabs, but the cells that had migrated were fixed with 5% glutaraldehyde solution to determine the number of migratory cells. The lower surfaces of the filters were stained with 0.25% trypan blue. Images of six different ×10 fields were captured from each membrane, and the number of migratory cells was counted. The mean of triplicate assays for each experimental condition was used. Similar inserts coated with Matrigel were used to evaluate the cell invasive potential in the invasion assay.

Flow Cytometry Analysis

Fluorescence-activated cell sorting (FACS) analysis was performed at 48 h post transfection. The cells were harvested, washed with cold PBS, fixed into 70% ethanol at −20°C for 24 h, stained with 50 μg/mL propidium iodide (PI) (4ABio, China), and analyzed using a FACS Calibur flow cytometer (BD Biosciences, USA). The results were analyzed using ModFit software (BD Biosciences, USA). Assays were conducted three independent times.

Western Blot Analysis

For western blot analyses, RIPA buffer containing protease inhibitors and phosphatase inhibitors (Roche) was used to prepare whole-cell lysates. Briefly, equal amounts of lysate were separated by SDS-PAGE and then transferred to polyvinylidene fluoride (PVDF) membranes (Millipore). After blocking with 5% BSA, the membranes were probed with anti-FOXK2 and anti-GAPDH (ab84761, 83286, and ab8425, Abcam, Cambridge, UK), followed by incubation with a horseradish peroxidase-conjugated secondary antibody goat-anti-mouse immunoglobulin G (IgG; 1:2,000) and goat-anti-rabbit IgG (1:3,000). Proteins were visualized by Image Reader LAS-4000 (Fujifilm) and analyzed by the Multi Gauge version (v.)3.2 software.

Generation of Stable Cell Lines

Recombinant lentiviral vectors containing miR-602 overexpression and irrelevant sequences were purchased from XIEBHC Biotechnology (Beijing, China). In addition to the lentivirus expression vectors, there was a luciferase and puromycin reporter gene driven by the EF1α promoter to indicate the infection efficiency in a timely manner. To construct lentiviral vectors, the precursor sequence for miR-602 and the irrelevant sequence (NC) were inserted into pHBLV-U6-MCS- EF1α-Luc-T2A-puromycin lentiviral vectors. The recombinant lentiviruses were packaged by co-transfection of HEK293T cells with pSPAX2 and pMD2.G with LipoFiter reagent. The supernatants with lentivirus particles were harvested at 48 and 72 h after transfection and filtered through 0.45-μm cellulose acetate filters (Millipore, USA). Recombinant lentiviruses were concentrated by ultracentrifugation. To establish stable cell lines, ESCC cells were transduced with lentivirus with an MOI of approximately 5 in the presence of 5 μg/mL polybrene. The supernatant was removed after 24 h and replaced with fresh complete culture medium. Infection efficiency was confirmed by RT-PCR at 96 h after infection, and the cells were selected with 2 μg/mL puromycin for 2 weeks.

Tumorigenicity and Metastasis Assay *In Vivo*

All animals received humane care in compliance with the Guide for the Care and Use of Laboratory Animals prepared by the Institute of Laboratory Animal Resources published by the NIH and according to the Animal Experiment Guidelines of Biomedical Research Institute. The effect of miR-602 on the tumorigenic and metastatic potential of ESCC cells was analyzed in subcutaneous and systemic metastasis *in vivo* models by right subcutaneous tissue and tail vein injection, respectively. For the subcutaneous model, 4- to 6-week-old BALB/c nude mice were injected subcutaneously in the right hip with 1×10^6 transfected cells. For the experimental metastasis *in vivo* model, transfected cancer cells (1×10^6 in 100 μL Hank's balanced salt solution [HBSS]) were directly injected into the tail vein. About 5 weeks later, tumor colonies in subcutaneous tissue were observed by H&E staining and histology examination. Bioluminescence images were collected to assess the growth and metastasis of implanted tumor cells. To quantify the *in vivo* bioluminescence signal, mice were anesthetized with isoflurane before *in vivo* imaging, and D-luciferin solution (*in vivo* imaging solutions, PerkinElmer, 150 mg/kg in PBS) was injected intravenously for systemic xenografts. Bioluminescence images were acquired with the IVIS Spectrum imaging system (PerkinElmer) 2–5 min after injection, and the captured images were quantified using the Living Image Software package (PerkinElmer/ Caliper Life Sciences) by measuring the photon flux (photons/s/cm^2/steradian) within a region of interest (ROI) drawn around the bioluminescence signal.

Antagomir Treatment

The antagomir and the miRNA NC were synthesized by RiboBio (Guangzhou, China) and implemented per the manufacturer's instructions. A 10-nmol miR-602 antagomir as well as the miRNA NC in 0.1 mL saline buffer were locally injected into the ESCC cell-forming tumor mass once every 5 days for 6 weeks. After the treatment, the ESCC cell-forming tumors were applied for the immunohistochemistry assay. The tumor size was monitored by measuring the length (L) and width (W) with calipers every 5 days, and the volumes were calculated using the formula $(L \times W^2)/2$. Mice were killed by cervical dislocation on day 42, and the tumors were excised and snap-frozen for protein and RNA extraction.

Evaluation of Immunohistochemical Staining

The section was de-paraffinized and boiled in 10 mM citrate buffer (pH 6.0) for antigen retrieval. Endogenous peroxidase was blocked by 3% H_2O_2. Slides were then blocked in serum, incubated with the indicated antibodies at 4°C overnight, incubated with anti-rabbit secondary antibody, and visualized with diaminobenzadine (Sigma). An NC experiment was also performed.

Statistical Analysis

All values reported in the paper are expressed as means ± SD, and all error bars represent the SD of the mean. Student's t test, the $\chi 2$ test,

and repeated-measures ANOVA were used to determine significance. The log rank test was used to analyze the effect of clinical variables and miRNAs on patients' OS. The Cox regression model was used to analyze the effect of the related factors on the survival time of patients with ESCC. ROC curves and the area under the ROC curve (AUC) were used to assess the feasibility of using serum miRNA as a diagnostic tool for detecting ESCC. The CpG unit methylation data of miR-602 from 18 pairs of ESCC tissues were used for stratified cluster analysis by Cluster 3.0 and Tree View software. Wilcoxon test was also conducted to compare the miR-602 expression between ESCC and normal esophageal cancer tissues. $p < 0.05$ was considered statistically significant. Statistical analyses were performed using SPSS 16.0 software (SPSS, USA).

SUPPLEMENTAL INFORMATION

Supplemental Information can be found online at https://doi.org/10.1016/j.ymthe.2019.07.006.

AUTHOR CONTRIBUTIONS

M.L., J.Y., and D.W. contributed to the analysis and interpretation of data and drafting of the manuscript. M.L., J.Y., D.W., and Y.N. contributed to the acquisition of data and technical support and revised the manuscript for important intellectual content. S.C., P.G., Z.Y., J.Z., C.Z., and Y.N. did the array and some experiments and contributed to technical support. P.G., J.Y., D.W., and M.L. contributed to the analysis and interpretation of data. Y.Z., W.H., and G.S. contributed to the study concept; design, analysis, and interpretation of data; and drafting of the manuscript. All authors read and approved the final manuscript.

CONFLICTS OF INTEREST

The authors declare no competing interests.

ACKNOWLEDGMENTS

This work was supported by grants from the National Natural Science Foundation of China (81402534), the Natural Science Foundation of Hebei province (H2019105026), the Young Top-Notch talent Project of Hebei province (JI201610), the Talent Project of Hebei province (A2016002090 and A201801005), the Medical Science Research and Key Project of Hebei province (ZD20140084), and the Academician Workstation Construction Special Project of Tangshan People's Hospital (199A77119H). No benefits in any form have been or will be received from a commercial party related directly or indirectly to the subject of this study.

REFERENCES

1. Chen, W., Zheng, R., Baade, P.D., Zhang, S., Zeng, H., Bray, F., Jemal, A., Yu, X.Q., and He, J. (2016). Cancer statistics in China, 2015. CA Cancer J. Clin. *66*, 115–132.
2. Li, X., Kleeman, S., Coburn, S.B., Fumagalli, C., Perner, J., Jammula, S., Pfeiffer, R.M., Orzolek, L., Hao, H., Taylor, P.R., et al. (2018). Selection and Application of Tissue microRNAs for Nonendoscopic Diagnosis of Barrett's Esophagus. Gastroenterology *155*, 771–783.e3.
3. Kim, S., Lee, E., Jung, J., Lee, J.W., Kim, H.J., Kim, J., Yoo, H.J., Lee, H.J., Chae, S.Y., Jeon, S.M., et al. (2018). microRNA-155 positively regulates glucose metabolism via PIK3R1-FOXO3a-cMYC axis in breast cancer. Oncogene *37*, 2982–2991.
4. Ren, L.L., Yan, T.T., Shen, C.Q., Tang, J.Y., Kong, X., Wang, Y.C., Chen, J., Liu, Q., He, J., Zhong, M., et al. (2018). The distinct role of strand-specific miR-514b-3p and miR-514b-5p in colorectal cancer metastasis. Cell Death Dis. *9*, 687.
5. Valeri, N., Braconi, C., Gasparini, P., Murgia, C., Lampis, A., Paulus-Hock, V., Hart, J.R., Ueno, L., Grivennikov, S.I., Lovat, F., et al. (2014). MicroRNA-135b promotes cancer progression by acting as a downstream effector of oncogenic pathways in colon cancer. Cancer Cell *25*, 469–483.
6. Sandbothe, M., Buurman, R., Reich, N., Greiwe, L., Vajen, B., Gürlevik, E., Schäffer, V., Eilers, M., Kühnel, F., Vaquero, A., et al. (2017). The microRNA-449 family inhibits TGF-β-mediated liver cancer cell migration by targeting SOX4. J. Hepatol. *66*, 1012–1021.
7. Zhang, J.X., Chen, Z.H., Chen, D.L., Tian, X.P., Wang, C.Y., Zhou, Z.W., Gao, Y., Xu, Y., Chen, C., Zheng, Z.S., et al. (2018). LINC01410-miR-532-NCF2-NF-kB feedback loop promotes gastric cancer angiogenesis and metastasis. Oncogene *37*, 2660–2675.
8. Ambros, V. (2003). MicroRNA pathways in flies and worms: growth, death, fat, stress, and timing. Cell *113*, 673–676.
9. Cao, J., Song, Y., Bi, N., Shen, J., Liu, W., Fan, J., Sun, G., Tong, T., He, J., Shi, Y., et al. (2013). DNA methylation-mediated repression of miR-886-3p predicts poor outcome of human small cell lung cancer. Cancer Res. *73*, 3326–3335.
10. Bandi, N., Zbinden, S., Gugger, M., Arnold, M., Kocher, V., Hasan, L., Kappeler, A., Brunner, T., and Vassella, E. (2009). miR-15a and miR-16 are implicated in cell cycle regulation in a Rb-dependent manner and are frequently deleted or down-regulated in non-small cell lung cancer. Cancer Res. *69*, 5553–5559.
11. Yanaihara, N., Caplen, N., Bowman, E., Seike, M., Kumamoto, K., Yi, M., Stephens, R.M., Okamoto, A., Yokota, J., Tanaka, T., et al. (2006). Unique microRNA molecular profiles in lung cancer diagnosis and prognosis. Cancer Cell *9*, 189–198.
12. Liu, B., Qu, J., Xu, F., Guo, Y., Wang, Y., Yu, H., and Qian, B. (2015). MiR-195 suppresses non-small cell lung cancer by targeting CHEK1. Oncotarget *6*, 9445–9456.
13. Ambros, V. (2004). The functions of animal microRNAs. Nature *431*, 350–355.
14. Mitchell, P.S., Parkin, R.K., Kroh, E.M., Fritz, B.R., Wyman, S.K., Pogosova-Agadjanyan, E.L., Peterson, A., Noteboom, J., O'Briant, K.C., Allen, A., et al. (2008). Circulating microRNAs as stable blood-based markers for cancer detection. Proc. Natl. Acad. Sci. USA *105*, 10513–10518.
15. He, Y., Lin, J., Kong, D., Huang, M., Xu, C., Kim, T.K., Etheridge, A., Luo, Y., Ding, Y., and Wang, K. (2015). Current State of Circulating MicroRNAs as Cancer Biomarkers. Clin. Chem. *61*, 1138–1155.
16. Hu, Z., Chen, X., Zhao, Y., Tian, T., Jin, G., Shu, Y., Chen, Y., Xu, L., Zen, K., Zhang, C., and Shen, H. (2010). Serum microRNA signatures identified in a genome-wide serum microRNA expression profiling predict survival of non-small-cell lung cancer. J. Clin. Oncol. *28*, 1721–1726.
17. Heneghan, H.M., Miller, N., Lowery, A.J., Sweeney, K.J., Newell, J., and Kerin, M.J. (2010). Circulating microRNAs as novel minimally invasive biomarkers for breast cancer. Ann. Surg. *251*, 499–505.
18. Tsujiura, M., Ichikawa, D., Komatsu, S., Shiozaki, A., Takeshita, H., Kosuga, T., Konishi, H., Morimura, R., Deguchi, K., Fujiwara, H., et al. (2010). Circulating microRNAs in plasma of patients with gastric cancers. Br. J. Cancer *102*, 1174–1179.
19. Ou, C., Sun, Z., Li, X., Li, X., Ren, W., Qin, Z., Zhang, X., Yuan, W., Wang, J., Yu, W., et al. (2017). MiR-590-5p, a density-sensitive microRNA, inhibits tumorigenesis by targeting YAP1 in colorectal cancer. Cancer Lett. *399*, 53–63.
20. Li, H., Zhou, Z.Q., Yang, Z.R., Tong, D.N., Guan, J., Shi, B.J., Nie, J., Ding, X.T., Li, B., Zhou, G.W., and Zhang, Z.Y. (2017). MicroRNA-191 acts as a tumor promoter by modulating the TET1-p53 pathway in intrahepatic cholangiocarcinoma. Hepatology *66*, 136–151.
21. Zhao, G., Jiang, T., Liu, Y., Huai, G., Lan, C., Li, G., Jia, G., Wang, K., and Yang, M. (2018). Droplet digital PCR-based circulating microRNA detection serve as a promising diagnostic method for gastric cancer. BMC Cancer *18*, 676.
22. Zhang, H., Yang, K., Ren, T., Huang, Y., Tang, X., and Guo, W. (2018). miR-16-5p inhibits chordoma cell proliferation, invasion and metastasis by targeting Smad3. Cell Death Dis. *9*, 680.
23. Chen, X., Luo, H., Li, X., Tian, X., Peng, B., Liu, S., Zhan, T., Wan, Y., Chen, W., Li, Y., et al. (2018). miR-331-3p Functions as an Oncogene by Targeting ST7L in Pancreatic Cancer. Carcinogenesis *39*, 1006–1015.

24. Gong, H., Song, L., Lin, C., Liu, A., Lin, X., Wu, J., Li, M., and Li, J. (2013). Downregulation of miR-138 sustains NF-κB activation and promotes lipid raft formation in esophageal squamous cell carcinoma. Clin. Cancer Res. *19*, 1083–1093.

25. Zhang, Q., Gan, H., Song, W., Chai, D., and Wu, S. (2018). MicroRNA-145 promotes esophageal cancer cells proliferation and metastasis by targeting SMAD5. Scand. J. Gastroenterol. *53*, 769–776.

26. Hamano, R., Miyata, H., Yamasaki, M., Kurokawa, Y., Hara, J., Moon, J.H., Nakajima, K., Takiguchi, S., Fujiwara, Y., Mori, M., and Doki, Y. (2011). Overexpression of miR-200c induces chemoresistance in esophageal cancers mediated through activation of the Akt signaling pathway. Clin. Cancer Res. *17*, 3029–3038.

27. Akanuma, N., Hoshino, I., Akutsu, Y., Murakami, K., Isozaki, Y., Maruyama, T., Yusup, G., Qin, W., Toyozumi, T., Takahashi, M., et al. (2014). MicroRNA-133a regulates the mRNAs of two invadopodia-related proteins, FSCN1 and MMP14, in esophageal cancer. Br. J. Cancer *110*, 189–198.

28. Zhang, C., Wang, C., Chen, X., Yang, C., Li, K., Wang, J., Dai, J., Hu, Z., Zhou, X., Chen, L., et al. (2010). Expression profile of microRNAs in serum: a fingerprint for esophageal squamous cell carcinoma. Clin. Chem. *56*, 1871–1879.

29. Komatsu, S., Ichikawa, D., Takeshita, H., Tsujiura, M., Morimura, R., Nagata, H., Kosuga, T., Iitaka, D., Konishi, H., Shiozaki, A., et al. (2011). Circulating microRNAs in plasma of patients with oesophageal squamous cell carcinoma. Br. J. Cancer *105*, 104–111.

30. Hirajima, S., Komatsu, S., Ichikawa, D., Takeshita, H., Konishi, H., Shiozaki, A., Morimura, R., Tsujiura, M., Nagata, H., Kawaguchi, T., et al. (2013). Clinical impact of circulating miR-18a in plasma of patients with oesophageal squamous cell carcinoma. Br. J. Cancer *108*, 1822–1829.

31. Kiuchi, J., Komatsu, S., Imamura, T., Nishibeppu, K., Shoda, K., Arita, T., Kosuga, T., Konishi, H., Shiozaki, A., Okamoto, K., et al. (2019). Low levels of tumour suppressor miR-655 in plasma contribute to lymphatic progression and poor outcomes in oesophageal squamous cell carcinoma. Mol. Cancer *18*, 2.

32. Godfrey, J.D., Morton, J.P., Wilczynska, A., Sansom, O.J., and Bushell, M.D. (2018). MiR-142-3p is downregulated in aggressive p53 mutant mouse models of pancreatic ductal adenocarcinoma by hypermethylation of its locus. Cell Death Dis. *9*, 644.

33. Anwar, S.L., Krech, T., Hasemeier, B., Schipper, E., Schweitzer, N., Vogel, A., Kreipe, H., Buurman, R., Skawran, B., and Lehmann, U. (2017). *hsa-mir-183* is frequently methylated and related to poor survival in human hepatocellular carcinoma. World J. Gastroenterol. *23*, 1568–1575.

34. Chen, K., Liu, M.X., Mak, C.S., Yung, M.M., Leung, T.H., Xu, D., Ngu, S.F., Chan, K.K., Yang, H., Ngan, H.Y., and Chan, D.W. (2018). Methylation-associated silencing of *miR-193a-3p* promotes ovarian cancer aggressiveness by targeting GRB7 and MAPK/ERK pathways. Theranostics *8*, 423–436.

35. Cui, X., Chen, X., Wang, W., Chang, A., Yang, L., Liu, C., Peng, H., Wei, Y., Liang, W., Li, S., et al. (2017). Epigenetic silencing of miR-203 in Kazakh patients with esophageal squamous cell carcinoma by MassARRAY spectrometry. Epigenetics *12*, 698–707.

36. Liang, G., and Weisenberger, D.J. (2017). DNA methylation aberrancies as a guide for surveillance and treatment of human cancers. Epigenetics *12*, 416–432.

37. Lu, Y.F., Yu, J.R., Yang, Z., Zhu, G.X., Gao, P., Wang, H., Chen, S.Y., Zhang, J., Liu, M.Y., Niu, Y., et al. (2018). Promoter hypomethylation mediated upregulation of MicroRNA-10b-3p targets FOXO3 to promote the progression of esophageal squamous cell carcinoma (ESCC). J. Exp. Clin. Cancer Res. *37*, 301.

38. Shan, L., Zhou, X., Liu, X., Wang, Y., Su, D., Hou, Y., Yu, N., Yang, C., Liu, B., Gao, J., et al. (2016). FOXK2 Elicits Massive Transcription Repression and Suppresses the Hypoxic Response and Breast Cancer Carcinogenesis. Cancer Cell *30*, 708–722.

39. Chen, S., Jiang, S., Hu, F., Xu, Y., Wang, T., and Mei, Q. (2017). Foxk2 inhibits non-small cell lung cancer epithelial-mesenchymal transition and proliferation through the repression of different key target genes. Oncol. Rep. *37*, 2335–2347.

40. Wang, B., Zhang, X., Wang, W., Zhu, Z., Tang, F., Wang, D., Liu, X., Zhuang, H., and Yan, X. (2018). Forkhead box K2 inhibits the proliferation, migration, and invasion of human glioma cells and predicts a favorable prognosis. OncoTargets Ther. *11*, 1067–1075.

41. van der Heide, L.P., Wijchers, P.J., von Oerthel, L., Burbach, J.P., Hoekman, M.F., and Smidt, M.P. (2015). FoxK2 is required for cellular proliferation and survival. J. Cell. Physiol. *230*, 1013–1023.

42. Liu, X., Wei, X., Niu, W., Wang, D., Wang, B., and Zhuang, H. (2018). Downregulation of FOXK2 is associated with poor prognosis in patients with gastric cancer. Mol. Med. Rep. *18*, 4356–4364.

43. Wang, W., Li, X., Lee, M., Jun, S., Aziz, K.E., Feng, L., Tran, M.K., Li, N., McCrea, P.D., Park, J.I., and Chen, J. (2015). FOXKs promote Wnt/β-catenin signaling by translocating DVL into the nucleus. Dev. Cell *32*, 707–718.